

Stokes flow through a twisted tube

By C. POZRIKIDIS

Department of Mechanical and Aerospace Engineering, University of California, San Diego,
La Jolla, CA 92093-0411, USA
cpozrikidis@ucsd.edu

(Received 18 February 2006 and in revised form 5 May 2006)

Pressure-driven flow through a tube with helical corrugations produced either by twisting a straight tube with arbitrary cross-section, or by embossing helical corrugations on a circular tube, or by inserting a helical fin inside a circular tube, is considered. The Stokes-flow problem is formulated in non-orthogonal curvilinear helical coordinates defined with respect to the helical pitch and azimuthal wavenumber, where the latter is determined by the tube cross-section rotational symmetry. In the first part of the paper, a perturbation analysis is carried out for a circular tube with small-amplitude sinusoidal corrugations, and the solutions of the first- and second-order perturbation problems are found by analytical methods. In the second part, an asymptotic analysis is performed for large-pitched helical corrugations and tubes with arbitrary cross-section, and the solutions of the zeroth-, first- and second-order problems are computed by finite-element methods for unidirectional and two-dimensional Stokes flow over the cross-sectional plane normal to the tube axis. The results illustrate the kinematic structure of the flow and demonstrate the dependence of the flow rate on the tube geometry.

1. Introduction

The practical desire to enhance heat transport and fluid mixing in a passive flow environment has motivated the design of pipes and tubes with internal partitions, fins, ridges and ribs (e.g. Garimella & Christensen 1995*a, b*). These obstructions are meant to disturb the otherwise rectilinear streamlines of the pipe flow and induce a rotational motion that promotes mixing and induces convective scalar transport. Applications can be found in high- and low-speed heat exchangers and in processing equipment encountered in the chemical and food industry. For example, the Kenics static mixer is assembled by inserting an array of helical segments into a circular tube (e.g. Galaktionov *et al.* 2001). Though such designs can lead to significant improvement in performance, side-effects and some practical concerns may occur. A poor construction may cause clogging and the onset of regions of recirculating flow that have an adverse effect on the transport rates. From a practical standpoint, the geometries may be hard to produce on a great variety of scales, especially on the small scale of microfluidics.

A generalized concept considers tubes with helical corrugations produced either by twisting a straight tube with a non-circular cross-section, or by embossing helical corrugations on a circular tube, as shown in figure 1. A circular tube with a helical internal fin falls into this category (figure 1*e*). Although flows through such tubes have been investigated in the laboratory, mainly with reference to enhanced heat transfer at high Reynolds numbers (e.g. Withers & Habdas 1974; Rainieri, Farina

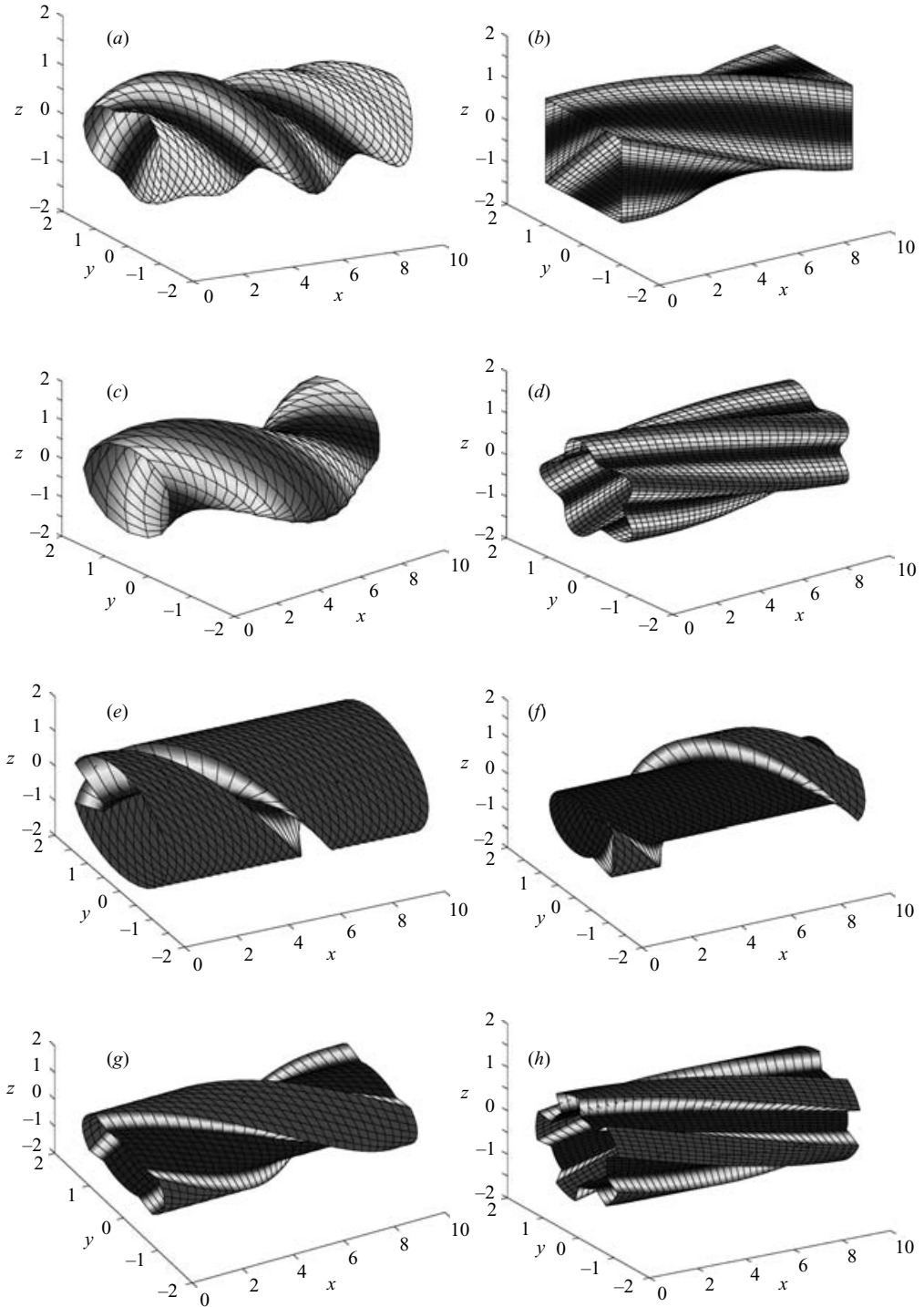


FIGURE 1. A periodically twisted tube with (a) arbitrary cross-section ($n = 1$); (b) square cross-section ($n = 4$); (c, d) circular cross-section with sinusoidal corrugations ($n = 1$ snake-like, and 5); (e) circular cross-section with a triangular indentation yielding an internal helical fin ($n = 1$); (f-h) circular contour with square indentations ($n = 1, 2$ and 5). The outside surface of the tube shown in (f) describes a single-screw extruder, and the outside surface of the tube shown in (g) describes a drill bit.

& Pagliarini 1996), a detailed hydrodynamic analysis is not available. A notable exception is Wang (2006) who carried out a perturbation analysis for twisted circular tubes with small-amplitude sinusoidal corrugations at low Reynolds numbers. His results demonstrate that there is an optimal pitch where the bulk rotation of the fluid in the core of the tube becomes maximum, optimizing laminar mixing.

Flow through twisted tubes should be distinguished from flow through spirally coiled tubes with a uniform cross-section whose centreline forms a helix. Such tubes are used in the nuclear and mechanical engineering industries for applications relating to heat exchange. The advantage of the coiled shape is that it offers a large transport surface area in a compact design, while allowing for a narrow distribution of residence times. The main hydrodynamic feature of flow through these curved tubes is the onset of secondary flow over the cross-section identified by Eustice (1910, 1911) and first analysed by Dean (1927, 1928), as reviewed by Berger, Talbot & Yao (1983) and Rennie (2004). Wang (1981) formulated the problem in centreline, normal and binormal coordinates and demonstrated the leading-order effect of the helical curvature and torsion for tubes with small cross-sectional shape – see also Germano (1982, 1989), Tuttle (1990) and Xie (1900). Numerical studies addressing the effect of torsion were performed by several authors (e.g. Liu & Masliyah 1993; Hüttl & Friedrich 2001). Notable is the work of Wang & Andrews (1995) who formulated the governing equations of Navier–Stokes flow in global helical coordinates and presented a comprehensive numerical study of the hydrodynamics for tubes with rectangular cross-sectional shape.

Flow through twisted and helical tubes falls in a more general category of flows with helical streamlines. Another member of this family is flow through an industrial single-screw extruder used in polymer and food processing. Several non-orthogonal helical coordinate systems have been proposed to study such flows, as reviewed by Yu & Hu (1997), and an appropriate choice must be made depending on the specific geometry of the problem under consideration. For example, the system of helical coordinates employed by Wang & Andrews (1995) is appropriate for flow through small-pitched coiled tubes. On the other hand, the system of helical coordinates developed by Tung & Laurence (1975) is appropriate for flow through long-pitched coiled tubes, single-screw extruders, and flow through twisted tubes with arbitrary cross-section presently considered.

In §2, the problem is formulated for arbitrary cross-sectional shapes. In §3, the chosen system of helical coordinates is introduced and the governing equations of Stokes flow are presented in these non-orthogonal curvilinear coordinates. In §4, a perturbation analysis for flow through a twisted circular tube with small-amplitude sinusoidal corrugations is presented, and the results are confirmed to coincide with those of Wang (2006) who used an alternative formulation in polar cylindrical coordinates. In addition, flow visualization and streamlines are displayed and discussed. In §5, an asymptotic expansion for large-pitched tubes with arbitrary cross-section is performed, and numerical solutions up to the second order are presented using finite-element methods for unidirectional and two-dimensional Stokes flow. Comparison of the asymptotic analysis with the perturbation analysis for a nearly circular tube will suggest that the large-pitch solution is accurate even for moderate wavenumbers.

2. Problem statement

We consider Stokes flow through a helically corrugated tube that arises by twisting a straight tube with arbitrary cross-section around its axis over the length of the

pitch, L . A point on the surface of the tube may be identified by its polar cylindrical coordinates, (x, σ, φ) , where the axial position, x , and meridional angle, φ , are regarded as independent variables. The distance from the tube centre is given by

$$\sigma = \Sigma(n\varphi - kx), \quad (2.1)$$

where $\Sigma(w)$ is a shape function with period 2π , the integer n is the meridional wavenumber for a tube with n -fold rotational cross-sectional symmetry, and the real number k is the axial wavenumber corresponding to the axial wave length or pitch, $L = 2\pi/k$. The helical geometry arises by twisting the tube cross-section at a particular location by an angle that depends linearly on the axial distance, x . Note that the tube cross-sectional geometries at x and $x + L$ are identical.

A twisted tube with arbitrary cross-section corresponding to $n = 1$ is illustrated in figure 1(a). A twisted tube with a square cross-section corresponding to $n = 4$ is illustrated in figure 1(b); the shape function in this case is

$$\Sigma(w) = \begin{cases} \frac{a}{\cos(w/4)} & \text{if } 0 < w < \pi, \\ \frac{a}{\sin(w/4)} & \text{if } \pi < w < 2\pi, \end{cases} \quad (2.2)$$

where a is half the tube side length. The shape function of a circular tube with sinusoidal corrugations is

$$\Sigma(w) = a + b \cos w, \quad (2.3)$$

where a is the mean tube radius and b is the amplitude of the corrugations (figure 1c, d). Other geometries arise by replacing the sinusoidal wave with a triangular or square wave, as shown in figure 1(e–h). For example, the shape function of a circular tube with square corrugations shown in figure 1(f–g) is

$$\Sigma(w) = \begin{cases} a + b & \text{if } |w| < \varphi_0, \\ a - b & \text{if otherwise,} \end{cases} \quad (2.4)$$

where φ_0 is a specified angle, and a, b are specified dimensions defining the inner and outer tube diameters. Matlab scripts that produce these shapes are available from the author on request.

3. Helical coordinates

A point inside the tube can be identified by the non-orthogonal helical curvilinear coordinates $(\hat{\sigma}, \hat{\varphi}, \hat{x})$, (figure 2). These are related to the cylindrical polar coordinates by

$$\sigma = \hat{\sigma}, \quad \varphi = \hat{\varphi} + \alpha\hat{x}, \quad x = \hat{x}, \quad (3.1)$$

and to the Cartesian coordinates by

$$x = \hat{x}, \quad y = \hat{\sigma} \cos(\hat{\varphi} + \alpha\hat{x}), \quad z = \hat{\sigma} \sin(\hat{\varphi} + \alpha\hat{x}), \quad (3.2)$$

where $\alpha \equiv k/n = 2\pi/(nL)$. The range of variation of the helical coordinates inside the tube over the length of one pitch is

$$0 < \hat{\sigma} < \Sigma(n\hat{\varphi}), \quad 0 < \hat{\varphi} < 2\pi, \quad 0 < \hat{x} < L. \quad (3.3)$$

Lines of constant $\hat{\varphi}$ on the tube surface correspond to a constant tube radius, $\hat{\sigma}$, as illustrated in figure 1.

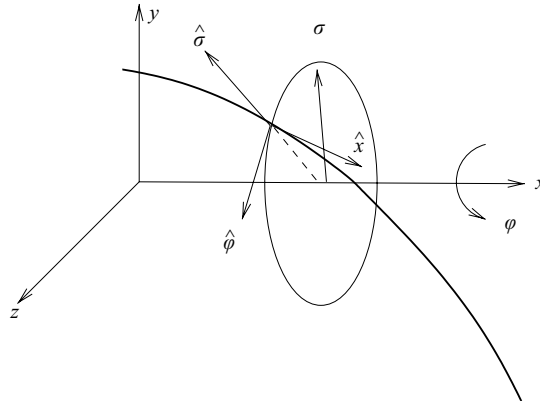


FIGURE 2. Definition of helical coordinates, $(\hat{x}, \hat{\sigma}, \hat{\varphi})$, in relation to the global Cartesian coordinates and polar cylindrical coordinates, (x, σ, φ) .

The helical coordinates $(\hat{\sigma}, \hat{\varphi}, \hat{x})$ defined above should be distinguished from the alternative helical coordinates $(\tilde{\sigma}, \tilde{\varphi}, \tilde{x})$ used by previous authors in the study of flow through a tube with a helical centreline and a circular or square cross-section (e.g. Wang & Andrews 1995; Manoussaki & Chadwick 2000), defined such that

$$\sigma = \tilde{\sigma}, \quad \varphi = \tilde{\varphi}, \quad x = \tilde{x} + \frac{1}{\alpha}\tilde{\varphi}, \tag{3.4}$$

and

$$x = \tilde{x} + \frac{1}{\alpha}\tilde{\varphi}, \quad y = \tilde{\sigma} \cos \tilde{\varphi}, \quad z = \tilde{\sigma} \sin \tilde{\varphi}. \tag{3.5}$$

These alternative helical coordinates are not suitable for helically twisted tubes that enclose the axis of revolution.

The covariant metric tensor of the chosen helical coordinates is

$$g_{ij} = \frac{\partial \mathbf{x}}{\partial \xi^i} \cdot \frac{\partial \mathbf{x}}{\partial \xi^j} = \begin{bmatrix} 1 & 0 & 0 \\ 0 & \hat{\sigma}^2 & \alpha \hat{\sigma}^2 \\ 0 & \alpha \hat{\sigma}^2 & 1 + \alpha^2 \hat{\sigma}^2 \end{bmatrix}, \tag{3.6}$$

where $\xi^1 = \hat{\sigma}$, $\xi^2 = \hat{\varphi}$ and $\xi^3 = \hat{x}$. The contravariant metric tensor is the inverse of the covariant tensor,

$$g^{ij} = \begin{bmatrix} 1 & 0 & 0 \\ 0 & \frac{1}{\hat{\sigma}^2} + \alpha^2 & -\alpha \\ 0 & -\alpha & 1 \end{bmatrix}. \tag{3.7}$$

A mean pressure gradient along the tube axis drives a three-dimensional pressure-driven flow. The fluid velocity can be resolved into components corresponding to the helical coordinates $(\hat{\sigma}, \hat{\varphi}, \hat{x})$,

$$\mathbf{u} = u_{\hat{\sigma}} \mathbf{e}_{\hat{\sigma}} + u_{\hat{\varphi}} \mathbf{e}_{\hat{\varphi}} + u_{\hat{x}} \mathbf{e}_{\hat{x}}, \tag{3.8}$$

where

$$\mathbf{e}_{\hat{\sigma}} = \frac{1}{\sqrt{g_{11}}} \left(\frac{\partial \mathbf{x}}{\partial \hat{\sigma}} \right)_{\hat{x}, \hat{\varphi}}, \quad \mathbf{e}_{\hat{\varphi}} = \frac{1}{\sqrt{g_{22}}} \left(\frac{\partial \mathbf{x}}{\partial \hat{\varphi}} \right)_{\hat{x}, \hat{\sigma}}, \quad \mathbf{e}_{\hat{x}} = \frac{1}{\sqrt{g_{33}}} \left(\frac{\partial \mathbf{x}}{\partial \hat{x}} \right)_{\hat{\sigma}, \hat{\varphi}}, \tag{3.9}$$

are position-dependent unit vectors. The cylindrical polar velocity components are related to the helical velocity components by

$$u_\sigma = u_{\hat{\sigma}}, \quad u_\varphi = u_{\hat{\varphi}} + \frac{\alpha \hat{\sigma}}{\sqrt{1 + \alpha^2 \hat{\sigma}^2}} u_{\hat{x}} = u_{\hat{\varphi}} + \alpha \hat{\sigma} u_x, \quad (3.10a, b)$$

$$u_x = \frac{1}{\sqrt{1 + \alpha^2 \hat{\sigma}^2}} u_{\hat{x}}. \quad (3.10c)$$

A key observation is that, if the flow is helically symmetric along the entire length of the tube, these velocity components are independent of \hat{x} , and only depend on $\hat{\sigma}$ and $\hat{\varphi}$. Moreover, since the flow is assumed to be fully developed, the axial derivative of the pressure is a constant,

$$-\left(\frac{\partial p}{\partial \hat{x}}\right)_{\hat{\sigma}, \hat{\varphi}} \equiv G, \quad (3.11)$$

where G is the negative of the streamwise pressure gradient.

The contravariant velocity components corresponding to the helical coordinates are given by

$$v^1 = \frac{u_{\hat{\sigma}}}{\sqrt{g_{11}}} = u_{\hat{\sigma}}, \quad v^2 = \frac{u_{\hat{\varphi}}}{\sqrt{g_{22}}} = \frac{u_{\hat{\varphi}}}{\hat{\sigma}}, \quad v^3 = \frac{u_{\hat{x}}}{\sqrt{g_{33}}} = \frac{u_{\hat{x}}}{\sqrt{1 + \alpha^2 \hat{\sigma}^2}} = u_x, \quad (3.12)$$

where u_x is the velocity component along the tube axis. Like the physical components, the contravariant components are independent of \hat{x} , and only depend on $\hat{\sigma}$ and $\hat{\varphi}$. The flow rate through a plane that is normal to the x -axis is given by

$$Q = \int_0^{2\pi} \int_0^{\Sigma(n\hat{\varphi})} u_x \hat{\sigma} \, d\hat{\sigma} \, d\hat{\varphi}. \quad (3.13)$$

The continuity equation for an incompressible fluid, $\nabla \cdot \mathbf{u} = 0$, requires

$$\frac{\partial v^i}{\partial \xi^i} + \left\{ \begin{matrix} i \\ j \ i \end{matrix} \right\} v^j = 0, \quad (3.14)$$

and the Stokes equation, $\nabla p = \mu \nabla^2 \mathbf{u}$ requires

$$g^{ij} \frac{\partial p}{\partial \xi^j} = \mu g^{kj} v_{,jk}^i, \quad (3.15)$$

where μ is the fluid viscosity, and

$$v_{,jk}^i = \frac{\partial^2 v^i}{\partial \xi^k \partial \xi^j} + \left\{ \begin{matrix} i \\ j \ l \end{matrix} \right\} \frac{\partial v^l}{\partial \xi^k} + \left\{ \begin{matrix} i \\ l \ k \end{matrix} \right\} \frac{\partial v^l}{\partial \xi^j} - \left\{ \begin{matrix} l \\ j \ k \end{matrix} \right\} \frac{\partial v^i}{\partial \xi^l} \\ + \left(\frac{\partial}{\partial \xi^k} \left\{ \begin{matrix} i \\ j \ l \end{matrix} \right\} + \left\{ \begin{matrix} i \\ m \ k \end{matrix} \right\} \left\{ \begin{matrix} m \\ j \ l \end{matrix} \right\} - \left\{ \begin{matrix} m \\ j \ k \end{matrix} \right\} \left\{ \begin{matrix} i \\ m \ l \end{matrix} \right\} \right) v^l \quad (3.16)$$

is the covariant second derivative (Wang 1981). The curly brackets signify the Christoffel symbol of the second kind defined as

$$\left\{ \begin{matrix} i \\ j \ k \end{matrix} \right\} \equiv g^{il} [jk, l] = \frac{\partial \xi^i}{\partial x^l} \frac{\partial}{\partial \xi^j} \left(\frac{\partial x^l}{\partial \xi^k} \right), \quad (3.17)$$

where x^i are the Cartesian coordinates, and

$$[jk, l] = \frac{1}{2} \left(\frac{\partial g_{lj}}{\partial \xi^k} + \frac{\partial g_{lk}}{\partial \xi^j} - \frac{\partial g_{jk}}{\partial \xi^l} \right) \quad (3.18)$$

is the Christoffel symbol of the first kind (Aris 1962). Substituting the aforementioned expressions, we find that the only non-zero Christoffel symbols of the second kind are (Tung & Laurence 1975)

$$\left. \begin{aligned} \left\{ \begin{matrix} 2 \\ 2 \ 1 \end{matrix} \right\} &= \frac{1}{\hat{\sigma}}, & \left\{ \begin{matrix} 2 \\ 3 \ 1 \end{matrix} \right\} &= \frac{\alpha}{\hat{\sigma}}, \\ \left\{ \begin{matrix} 1 \\ 2 \ 2 \end{matrix} \right\} &= -\hat{\sigma}, & \left\{ \begin{matrix} 1 \\ 3 \ 2 \end{matrix} \right\} &= -\alpha\hat{\sigma}, & \left\{ \begin{matrix} 2 \\ 1 \ 2 \end{matrix} \right\} &= \frac{1}{\hat{\sigma}}, \\ \left\{ \begin{matrix} 1 \\ 2 \ 3 \end{matrix} \right\} &= -\alpha\hat{\sigma}, & \left\{ \begin{matrix} 1 \\ 3 \ 3 \end{matrix} \right\} &= -\alpha^2\hat{\sigma}, & \left\{ \begin{matrix} 2 \\ 1 \ 3 \end{matrix} \right\} &= \frac{\alpha}{\hat{\sigma}}. \end{aligned} \right\} \quad (3.19)$$

Substituting these expressions into the continuity equation and setting the derivative with respect to ξ^3 equal to zero, we find

$$\frac{\partial u_{\hat{\sigma}}}{\partial \hat{\sigma}} + \frac{\partial}{\partial \hat{\varphi}} \left(\frac{u_{\hat{\varphi}}}{\hat{\sigma}} \right) + \left\{ \begin{matrix} 2 \\ 1 \ 2 \end{matrix} \right\} u_{\hat{\sigma}} = \frac{1}{\hat{\sigma}} \left(\frac{\partial(\hat{\sigma} u_{\hat{\sigma}})}{\partial \hat{\sigma}} + \frac{\partial u_{\hat{\varphi}}}{\partial \hat{\varphi}} \right) = 0, \quad (3.20)$$

which is the usual continuity equation in a plane normal to the x -axis corresponding to a fixed value of \hat{x} . Thus, the two-dimensional velocity field comprised of the helical velocity components in a plane normal to the x -axis is solenoidal and may be described in terms of a streamfunction. It is instructive to re-derive this expression departing from the continuity equation in cylindrical polar coordinates,

$$\frac{1}{\sigma} \frac{\partial(\sigma u_{\sigma})}{\partial \sigma} + \frac{\partial}{\partial \varphi} \left(\frac{u_{\varphi}}{\sigma} \right) + \frac{\partial u_x}{\partial x} = 0. \quad (3.21)$$

Using (3.10c), we find

$$\frac{1}{\sigma} \frac{\partial(\sigma u_{\hat{\sigma}})}{\partial \sigma} + \frac{\partial}{\partial \varphi} \left(\frac{u_{\hat{\varphi}} + \alpha \hat{\sigma} u_x}{\sigma} \right) + \frac{\partial u_x}{\partial x} = 0. \quad (3.22)$$

Since u_x depends only on $\hat{\varphi} = \varphi - \alpha x$,

$$\frac{\partial u_x}{\partial \varphi} = \frac{\partial u_x}{\partial \hat{\varphi}}, \quad \frac{\partial u_x}{\partial x} = -\alpha \frac{\partial u_x}{\partial \hat{\varphi}}. \quad (3.23)$$

Substituting these expressions into (3.22), we recover precisely (3.20).

The $\hat{\sigma}$ component of the Stokes equation reduces to

$$\frac{1}{\mu} \frac{\partial p}{\partial \hat{\sigma}} = \frac{\partial}{\partial \hat{\sigma}} \left(\frac{1}{\hat{\sigma}} \frac{\partial}{\partial \hat{\sigma}} (\hat{\sigma} u_{\hat{\sigma}}) \right) + \frac{1}{\hat{\sigma}^2} \frac{\partial^2 u_{\hat{\sigma}}}{\partial \hat{\varphi}^2} - \frac{2}{\hat{\sigma}^2} \frac{\partial u_{\hat{\varphi}}}{\partial \hat{\varphi}} + \alpha F_{\hat{\sigma}}, \quad (3.24)$$

where

$$F_{\hat{\sigma}} \equiv \alpha \frac{\partial^2 u_{\hat{\sigma}}}{\partial \hat{\varphi}^2} - \frac{2}{\hat{\sigma}} \frac{\partial u_x}{\partial \hat{\varphi}}, \quad (3.25)$$

the $\hat{\varphi}$ component reduces to

$$\frac{1}{\mu} \frac{1}{\hat{\sigma}} \frac{\partial p}{\partial \hat{\varphi}} = \frac{\partial}{\partial \hat{\sigma}} \left(\frac{1}{\hat{\sigma}} \frac{\partial}{\partial \hat{\sigma}} (\hat{\sigma} u_{\hat{\varphi}}) \right) + \frac{1}{\hat{\sigma}^2} \frac{\partial^2 u_{\hat{\varphi}}}{\partial \hat{\varphi}^2} + \frac{2}{\hat{\sigma}^2} \frac{\partial u_{\hat{\sigma}}}{\partial \hat{\varphi}} + \alpha F_{\hat{\varphi}}, \quad (3.26)$$

where

$$F_{\hat{\varphi}} = \alpha \frac{\partial^2 u_{\hat{\varphi}}}{\partial \hat{\varphi}^2} + 2 \frac{\partial u_x}{\partial \hat{\sigma}} - \frac{1}{\mu} \hat{\sigma} \left(G + \alpha \frac{\partial p}{\partial \hat{\varphi}} \right), \quad (3.27)$$

and the \hat{x} component of the Stokes equation reduces to

$$-\frac{G}{\mu} = \frac{1}{\hat{\sigma}} \frac{\partial}{\partial \hat{\sigma}} \left(\hat{\sigma} \frac{\partial u_x}{\partial \hat{\sigma}} \right) + \frac{1}{\hat{\sigma}^2} \frac{\partial^2 u_x}{\partial \hat{\phi}^2} + \alpha F_{\hat{x}}, \quad (3.28)$$

where

$$F_{\hat{x}} \equiv \alpha \frac{\partial^2 u_x}{\partial \hat{\phi}^2} + \frac{1}{\mu} \frac{\partial p}{\partial \hat{\phi}} \quad (3.29)$$

(Tung & Laurence 1975). A simple way to derive these equations is by transforming the Stokes equations in polar cylindrical coordinates using (3.10) and the chain rule. In the case of a straight tube, $\alpha=0$, we recover the Stokes equations written in cylindrical polar coordinates. In Stokes flow, the pressure is a harmonic function, $\nabla^2 p = 0$. In light of the helical symmetry, the covariant components of the pressure gradient are given by

$$q_1 = \frac{\partial p}{\partial \hat{\sigma}}, \quad q_2 = \frac{\partial p}{\partial \hat{\phi}}, \quad q_3 = \frac{\partial p}{\partial \hat{x}} = -G. \quad (3.30)$$

The contravariant components arise from the relation $q^i = g^{ij} q_j$,

$$q^1 = q_1, \quad q^2 = \left(\frac{1}{\hat{\sigma}^2} + \alpha^2 \right) q_2 + \alpha G, \quad q^3 = -\alpha q_2 - G. \quad (3.31)$$

Laplace's equation for in general non-orthogonal curvilinear coordinates reads

$$\nabla^2 p = \frac{1}{\sqrt{g}} \frac{\partial}{\partial v^i} (\sqrt{g} q^i) = 0, \quad (3.32)$$

where g is the determinant of the covariant matrix tensor. In our case, $g = \hat{\sigma}^2$, the term involving derivatives with respect to \hat{x} is zero, and we find

$$\frac{1}{\hat{\sigma}} \frac{\partial (\hat{\sigma} q^1)}{\partial \hat{\sigma}} + \frac{\partial q^2}{\partial \hat{\phi}} = \frac{1}{\hat{\sigma}} \frac{\partial}{\partial \hat{\sigma}} \left(\hat{\sigma} \frac{\partial p}{\partial \hat{\sigma}} \right) + \left(\frac{1}{\hat{\sigma}^2} + \alpha^2 \right) \frac{\partial^2 p}{\partial \hat{\phi}^2} = 0, \quad (3.33)$$

which shows that the pressure distribution in an axial plane is harmonic only when $\alpha = 0$.

In the case of flow through a circular tube, the governing equations are satisfied by the Poiseuille flow profile for any value of α , yielding

$$\left. \begin{aligned} u_{\hat{\sigma}} &= 0, & u_{\hat{\phi}} &= -\alpha \hat{\sigma} \frac{G}{4\mu} (a^2 - \hat{\sigma}^2), \\ u_x &= \frac{G}{4\mu} (a^2 - \hat{\sigma}^2), & p &= -G\hat{x} + P_0, \end{aligned} \right\} \quad (3.34)$$

where P_0 is an inconsequential constant. In this case, there is no advantage to using helical coordinates in place of the natural cylindrical polar coordinates.

4. Small-amplitude sinusoidal corrugations around the circular shape

Consider flow through a circular tube of radius a with small-amplitude sinusoidal corrugations described by the shape function

$$\Sigma(w) = a(1 + \epsilon \cos w), \quad (4.1)$$

where ϵ is a dimensionless number that is much smaller than unity. This flow was studied recently by Wang (2006) using a formulation in polar cylindrical coordinates.

In the helical coordinates employed here, the velocity and pressure fields may be expanded in the perturbation series

$$\left. \begin{aligned} u_{\hat{\sigma}} &= \epsilon u_{\hat{\sigma}}^{(1)} + \epsilon^2 u_{\hat{\sigma}}^{(2)} + \cdots, \\ u_{\hat{\phi}} &= -\alpha \hat{\sigma} \frac{G}{4\mu} (a^2 - \hat{\sigma}^2) + \epsilon u_{\hat{\phi}}^{(1)} + \epsilon^2 u_{\hat{\phi}}^{(2)} + \cdots, \\ u_x &= \frac{G}{4\mu} (a^2 - \hat{\sigma}^2) + \epsilon u_x^{(1)} + \epsilon^2 u_x^{(2)} + \cdots, \\ p &= -G\hat{x} + \epsilon p^{(1)} + \epsilon^2 p^{(2)} + \cdots. \end{aligned} \right\} \quad (4.2)$$

Note that the zeroth-order component of $u_{\hat{\phi}}$ is non-zero according to (3.10). The no-slip and no-penetration boundary conditions require that the velocity components $u_{\hat{\sigma}}$, $u_{\hat{\phi}}$, and u_x are all zero around the tube surface located at

$$\hat{\sigma} = a(1 + \epsilon \cos(n\hat{\phi})). \quad (4.3)$$

Substituting the perturbation expansions and linearizing, we derive the boundary conditions

$$\left. \begin{aligned} u_{\hat{\sigma}}^{(1)}(\hat{\sigma} = a) &= 0, \quad u_{\hat{\phi}}^{(1)}(\hat{\sigma} = a) = -\alpha \frac{Ga^3}{2\mu} \cos(n\hat{\phi}), \\ u_x^{(1)}(\hat{\sigma} = a) &= \frac{Ga^2}{2\mu} \cos(n\hat{\phi}). \end{aligned} \right\} \quad (4.4)$$

Motivated by these functional forms, we write

$$\left. \begin{aligned} u_{\hat{\sigma}}^{(1)} &= U_{\hat{\sigma}}(\hat{\sigma}) \sin(n\hat{\phi}), \quad u_{\hat{\phi}}^{(1)} = U_{\hat{\phi}}(\hat{\sigma}) \cos(n\hat{\phi}), \\ u_x^{(1)} &= U_x(\hat{\sigma}) \cos(n\hat{\phi}), \quad p^{(1)} = P(\hat{\sigma}) \sin(n\hat{\phi}). \end{aligned} \right\} \quad (4.5)$$

The boundary conditions at the tube surface require

$$U_{\hat{\sigma}}(a) = 0, \quad U_{\hat{\phi}}(a) = -\alpha \frac{Ga^3}{2\mu}, \quad U_x(a) = \frac{Ga^2}{2\mu}, \quad (4.6)$$

and the regularity condition at the centreline requires $U_{\hat{\sigma}}(0) = 0$ and $U_{\hat{\phi}}(0) = 0$.

Substituting these expressions in the continuity equation (3.20), we find

$$\frac{d(\hat{\sigma} U_{\hat{\sigma}})}{d\hat{\sigma}} - n U_{\hat{\phi}} = 0. \quad (4.7)$$

Substituting the expression for the pressure in (3.33), we derive the ordinary differential equation

$$\mathcal{D}^2 \langle P \rangle = 0, \quad (4.8)$$

where

$$\mathcal{D}^2 \equiv \frac{1}{\hat{\sigma}} \frac{d}{d\hat{\sigma}} \left(\hat{\sigma} \frac{d}{d\hat{\sigma}} \right) - \left(\frac{n^2}{\sigma^2} + k^2 \right) \quad (4.9)$$

is the modified Bessel operator. Substituting further these expressions into the three components of the Stokes equation, (3.24), (3.26) and (3.28), we find

$$\tilde{\mathcal{D}}^2 \langle U_{\hat{\sigma}} \rangle + \frac{2n}{\hat{\sigma}^2} U_{\hat{\phi}} + \frac{2k}{\hat{\sigma}} U_x = \frac{1}{\mu} \frac{dP}{d\hat{\sigma}}, \quad (4.10)$$

$$\tilde{\mathcal{D}}^2 \langle U_{\hat{\phi}} \rangle + \frac{2n}{\hat{\sigma}^2} U_{\hat{\sigma}} + 2\alpha \frac{dU_x}{d\hat{\sigma}} = \frac{1 + \alpha^2 \sigma^2}{\mu \hat{\sigma}} n P, \quad (4.11)$$

$$\mathcal{D}^2 \langle U_x \rangle = -\frac{k}{\mu} P, \quad (4.12)$$

where

$$\tilde{\mathcal{D}}^2 \equiv \mathcal{D}^2 - \frac{1}{\hat{\sigma}^2} = \frac{1}{\hat{\sigma}} \frac{d}{d\hat{\sigma}} \left(\hat{\sigma} \frac{d}{d\hat{\sigma}} \right) - \left(\frac{n^2 + 1}{\sigma^2} + k^2 \right). \quad (4.13)$$

The admissible regular solution of (4.8) is

$$P = -\frac{Ga}{4} AI_n(k\hat{\sigma}), \quad (4.14)$$

where I_n is a modified Bessel function, and A is a dimensionless constant. Substituting this expression into (4.12), we find

$$\mathcal{D}^2 \langle U_x \rangle = \frac{Gka}{4\mu} AI_n(k\hat{\sigma}). \quad (4.15)$$

The solution is given by

$$U_x = \frac{Ga^2}{4\mu} \left[BI_n(k\hat{\sigma}) + \frac{A}{ka} \mathcal{F}(k\hat{\sigma}) \right], \quad (4.16)$$

where B is a new dimensionless constant, and the function $\mathcal{F}(R)$ satisfies the inhomogeneous Bessel equation

$$\frac{1}{R} \frac{d}{dR} \left(R \frac{d\mathcal{F}}{dR} \right) - \left(\frac{n^2}{R^2} + 1 \right) \mathcal{F} = I_n(R). \quad (4.17)$$

A particular solution of (4.17) is $\mathcal{F} = \frac{1}{2} RI_{n+1}(R)$. Substituting this expression into (4.16), we find

$$U_x = \frac{Ga^2}{4\mu} \left[BI_n(k\hat{\sigma}) + A \frac{\hat{\sigma}}{2a} I_{n+1}(k\hat{\sigma}) \right]. \quad (4.18)$$

Solving (4.7) for $U_{\hat{\varphi}}$ and substituting the result into (4.10), we find

$$\tilde{\mathcal{D}}^2 \langle U_{\hat{\sigma}} \rangle + \frac{2}{\hat{\sigma}^2} \frac{d(\hat{\sigma} \hat{U}_{\hat{\sigma}})}{d\hat{\sigma}} = -\frac{2k}{\hat{\sigma}} U_x + \frac{1}{\mu} \frac{dP}{d\hat{\sigma}}. \quad (4.19)$$

Substituting the preceding expressions and simplifying, we derive the ordinary differential equation

$$\begin{aligned} \frac{d^2 U_{\hat{\sigma}}}{d\hat{\sigma}^2} + \frac{3}{\hat{\sigma}} \frac{dU_{\hat{\sigma}}}{d\hat{\sigma}} - \left(\frac{n^2 - 1}{\hat{\sigma}^2} + k^2 \right) U_{\hat{\sigma}} &= \frac{1}{\hat{\sigma}} \mathcal{D}^2 \langle \hat{\sigma} U_{\hat{\sigma}} \rangle \\ &= -\frac{Gak}{4\mu} \left[(2kaB + An) \frac{I_n(k\hat{\sigma})}{k\hat{\sigma}} + 2AI_{n+1}(k\hat{\sigma}) \right]. \end{aligned} \quad (4.20)$$

The solution is

$$U_{\hat{\sigma}} = \frac{Ga^2}{4\mu} \left[C \frac{I_n(k\hat{\sigma})}{k\hat{\sigma}} - \frac{2kaB + An}{2ka} I_{n+1}(k\hat{\sigma}) - \frac{2A}{ka} \frac{1}{k\hat{\sigma}} \mathcal{G}(k\hat{\sigma}) \right], \quad (4.21)$$

where C is a new dimensionless constant, and the function $\mathcal{G}(R)$ satisfies the differential equation

$$\frac{1}{R} \frac{d}{dR} \left(R \frac{d\mathcal{G}}{dR} \right) - \left(\frac{n^2}{R^2} + 1 \right) \mathcal{G} = RI_{n+1}(R). \quad (4.22)$$

A solution of (4.22) is

$$\mathcal{G} = \frac{1}{4} R [RI_n(R) - 2(n+1)I_{n+1}(R)]. \quad (4.23)$$

Substituting (4.23) into (4.21), we find

$$U_{\hat{\sigma}} = \frac{Ga^2}{4\mu} \left[C \frac{I_n(k\hat{\sigma})}{k\hat{\sigma}} - BI_{n+1}(k\hat{\sigma}) - \frac{A}{2ka} (k\hat{\sigma} I_n(k\hat{\sigma}) - (n+2)I_{n+1}(k\hat{\sigma})) \right]. \quad (4.24)$$

Once again using (4.7), we find

$$U_{\hat{\varphi}} = \frac{1}{n} \frac{d(\hat{\sigma} U_{\hat{\sigma}})}{d\hat{\sigma}} = \frac{Ga^2}{4\mu} \left[C \left(\frac{I_n(k\hat{\sigma})}{k\hat{\sigma}} + \frac{I_{n+1}(k\hat{\sigma})}{n} \right) - B(\alpha\hat{\sigma} I_n(k\hat{\sigma}) - I_{n+1}(k\hat{\sigma})) - \frac{A}{2ka} \left(n+2 + \frac{k^2\hat{\sigma}^2}{n} \right) I_{n+1}(k\hat{\sigma}) \right]. \quad (4.25)$$

The physical meridional velocity component is given by

$$U_{\varphi} = U_{\hat{\varphi}} + \alpha\hat{\sigma} U_x \\ = \frac{Ga^2}{4\mu} \left[C \left(\frac{I_n(k\hat{\sigma})}{k\hat{\sigma}} + \frac{I_{n+1}(k\hat{\sigma})}{n} \right) + BI_{n+1}(k\hat{\sigma}) - \frac{A}{2ka} (n+2)I_{n+1}(k\hat{\sigma}) \right]. \quad (4.26)$$

The boundary condition $U_x(a) = Ga^2/(2\mu)$ requires

$$2BI_n(ka) + AI_{n+1}(ka) = 4, \quad (4.27)$$

the boundary condition $U_{\hat{\sigma}}(a) = 0$ requires

$$CI_n(ka) - BkaI_{n+1}(ka) - \frac{1}{2}A(kaI_n(ka) - (n+2)I_{n+1}(ka)) = 0, \quad (4.28)$$

and the boundary condition $U_{\hat{\varphi}}(a) = -\alpha Ga^3/(2\mu)$ or $U_{\varphi} = 0$ requires

$$C2(I_n(ka) + \alpha I_{n+1}(ka)) + B2kaI_{n+1}(ka) - A(n+2)I_{n+1}(ka) = 0. \quad (4.29)$$

The last three equations provide us with a linear system for the determination of the three dimensionless coefficients, A , B and C .

Figure 3(a) shows the first-order velocity vector field in a plane normal to the x -axis for $n = 3$ and $ka = \pi$. The dotted line represents the actual tube contour for $\epsilon = 0.05$. Note that, because of the helical symmetry, the displayed vector field is rotated as a whole along the tube axis at a rate that is determined by the pitch. Figure 3(b) shows coiled and spiralling streamlines for $\epsilon = 0.1$, generated by integrating the zeroth- and first-order velocity vector fields. The coiled streamlines exhibit a periodicity that allows them to explore a large part of the tube cross-section and thereby enhance laminar mixing.

The second-order perturbation velocity and pressure fields consist of a periodic sinusoidal component with respect to $\hat{\varphi}$, and a mean component that is independent of $\hat{\varphi}$, given by

$$\left. \begin{aligned} \mathcal{U}_{\hat{\sigma}}(\hat{\sigma}) &= \frac{1}{2\pi} \int_0^{2\pi} u_{\hat{\sigma}}^{(2)} d\hat{\varphi}, & \mathcal{U}_{\hat{\varphi}}(\hat{\sigma}) &= \frac{1}{2\pi} \int_0^{2\pi} u_{\hat{\varphi}}^{(2)} d\hat{\varphi}, \\ \mathcal{U}_x(\hat{\sigma}) &= \frac{1}{2\pi} \int_0^{2\pi} u_x^{(2)} d\hat{\varphi}, & \mathcal{P} &= \frac{1}{2\pi} \int_0^{2\pi} p^{(2)} d\hat{\varphi}. \end{aligned} \right\} \quad (4.30)$$

Integrating the continuity equation (3.20) with respect to $\hat{\varphi}$, and repeating for the three components of the Stokes equation (3.24), (3.26), (3.28), and the pressure

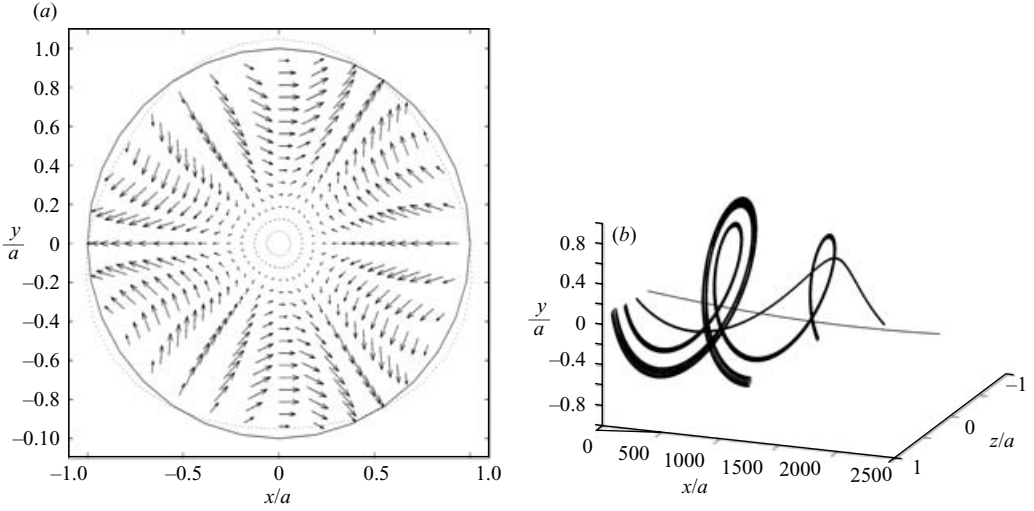


FIGURE 3. (a) Velocity vector field in a cross-sectional plane for $n = 3$ and $ka = \pi$. The dotted line represents the actual tube contour for $\epsilon = 0.05$. (b) Coiled and spiralling streamlines for $\epsilon = 0.1$, as predicted by the first-order analysis.

equation (4.14), we find

$$\left. \begin{aligned} \frac{1}{\hat{\sigma}} \frac{d(\hat{\sigma} \mathcal{U}_{\hat{\sigma}})}{d\hat{\sigma}} &= 0, & \frac{1}{\mu} \frac{d\mathcal{P}}{d\hat{\sigma}} &= \frac{d}{d\hat{\sigma}} \left(\frac{1}{\hat{\sigma}} \frac{d}{d\hat{\sigma}} (\hat{\sigma} \mathcal{U}_{\hat{\sigma}}) \right), \\ \frac{d}{d\hat{\sigma}} \left(\frac{1}{\hat{\sigma}} \frac{d}{d\hat{\sigma}} (\hat{\sigma} \mathcal{U}_{\hat{\varphi}}) \right) + 2\alpha \frac{d\mathcal{U}_x}{d\hat{\sigma}} &= 0, & \frac{1}{\hat{\sigma}} \frac{d}{d\hat{\sigma}} \left(\hat{\sigma} \frac{d\mathcal{U}_x}{d\hat{\sigma}} \right) &= 0, \\ \frac{1}{\hat{\sigma}} \frac{d}{d\hat{\sigma}} \left(\hat{\sigma} \frac{d\mathcal{P}}{d\hat{\sigma}} \right) &= 0. \end{aligned} \right\} \quad (4.31)$$

The boundary conditions are

$$\left. \begin{aligned} (\mathcal{U}_{\hat{\sigma}})_{\hat{\sigma}=a} &= 0, \\ (\mathcal{U}_{\hat{\varphi}})_{\hat{\sigma}=a} &= -\frac{1}{2} \left[3\alpha \frac{Ga^3}{4\mu} + a \left(\frac{dU_{\hat{\varphi}}}{d\sigma} \right)_{\hat{\sigma}=a} \right], \\ (\mathcal{U}_x)_{\hat{\sigma}=a} &= \frac{1}{2} \left[\frac{Ga^2}{4\mu} - a \left(\frac{dU_x}{d\sigma} \right)_{\hat{\sigma}=a} \right]. \end{aligned} \right\} \quad (4.32)$$

The solution of the second-order problem is readily found to be

$$\mathcal{U}_{\hat{\sigma}}(\hat{\sigma}) = 0, \quad \mathcal{U}_{\hat{\varphi}}(\hat{\sigma}) = (\mathcal{U}_{\hat{\varphi}})_{\hat{\sigma}=a} \frac{\hat{\sigma}}{a}, \quad \mathcal{U}_x(\hat{\sigma}) = (\mathcal{U}_x)_{\hat{\sigma}=a}. \quad (4.33)$$

The physical azimuthal velocity component is given by

$$\mathcal{U}_{\phi}(\hat{\sigma}) = \mathcal{U}_{\hat{\varphi}}(\hat{\sigma}) + \alpha \hat{\sigma} \mathcal{U}_x(\hat{\sigma}) = \Omega \hat{\sigma}, \quad (4.34)$$

where

$$\Omega = \frac{1}{a} \mathcal{U}_{\hat{\varphi}}(\hat{\sigma} = a) + \alpha \mathcal{U}_x(\hat{\sigma} = a) \quad (4.35)$$

is the angular velocity of rotation around the tube axis. The total flow rate through

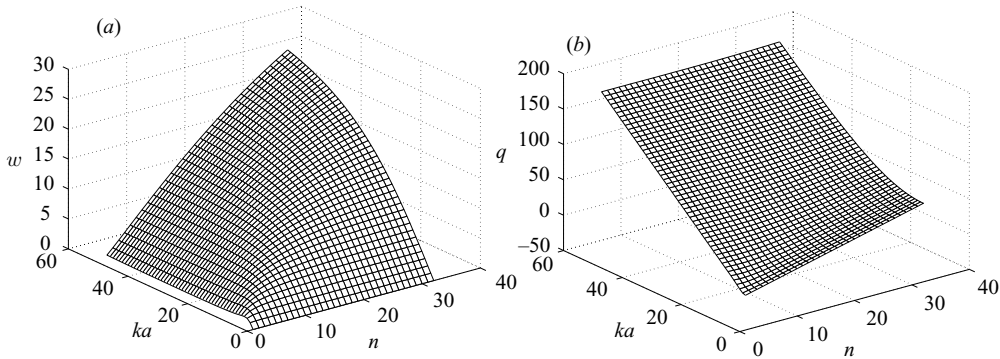


FIGURE 4. (a) Reduced angular velocity, $w \equiv 4\mu\Omega/(Ga)$, and (b) perturbation flow rate coefficient q , plotted as functions of n and ka .

a plane that is normal to the x -axis is given by

$$\begin{aligned}
 Q &= \int_0^{2\pi} \int_0^{a(1+\epsilon \cos(n\hat{\varphi}))} u_x \hat{\sigma} \, d\hat{\sigma} \, d\hat{\varphi} \\
 &= \int_0^{2\pi} \int_0^{a(1+\epsilon \cos(n\hat{\varphi}))} \left[\frac{G}{4\mu} (a^2 - \hat{\sigma}^2) + \epsilon U_x(\hat{\sigma}) \cos(n\hat{\varphi}) + \epsilon^2 u_x^{(2)} + \dots \right] \hat{\sigma} \, d\hat{\sigma} \, d\hat{\varphi} \\
 &= \frac{G\pi a^4}{8\mu} [1 - \epsilon^2 q + \dots], \tag{4.36}
 \end{aligned}$$

where

$$q = \frac{4\mu}{Ga} \left(\frac{dU_x}{d\sigma} \right)_{\hat{\sigma}=a} - 3 \tag{4.37}$$

is the second-order fractional decrease in the flow rate.

Figure 4(a) shows a graph of the dimensionless angular velocity, $w \equiv 4\mu\Omega/(Ga)$, plotted as a function of n and ka . As $ka \rightarrow 0$, $w \simeq ka$, independent of n , and as $ka \rightarrow \infty$, $w \simeq 3n/(2ka)$. Wang (2006) noted that, for a specified value of n , the angular velocity reaches a maximum at a certain value of ka representing the optimal pitch for fluid rotation around the tube axis.

Figure 4(b) shows a graph of the flow rate coefficient q , plotted as a function of n and ka . As $ka \rightarrow 0$, $q \simeq 2n - 3 + O(k^2 a^2)$, where the leading-order term expresses the effect of the sinusoidal corrugations in unidirectional flow. Thus, the first correction to the flow rate is quadratic with respect to the reduced wavenumber, ka . On the other hand, as $ka \rightarrow \infty$, $q \simeq 4ka - 3$, independent of n . Wang (2006) observed that q may obtain negative values when $n = 1$ for small values of ka , which means that the corrugations may actually reduce the energy required to drive the flow. Physically, the effective increase in the tube cross-sectional area overcompensates for the elevated drag due to the increased surface area.

5. Large pitch

Consider flow through a helically corrugated tube with arbitrary cross-section, in the limit as the dimensionless parameter,

$$\beta \equiv \alpha a = \frac{ka}{n} = \frac{2\pi a}{n L} \tag{5.1}$$

is small, where a is the typical cross-sectional tube size. The velocity and pressure fields may be expanded in the perturbation series

$$\left. \begin{aligned} u_{\hat{\sigma}} &= \beta u_{\hat{\sigma}}^{(1)} + \beta^2 u_{\hat{\sigma}}^{(2)} + \dots, \\ u_{\hat{\phi}} &= \beta u_{\hat{\phi}}^{(1)} + \beta^2 u_{\hat{\phi}}^{(2)} + \dots, \\ u_x &= u_x^{(0)} + \beta u_x^{(1)} + \beta^2 u_x^{(2)} + \dots, \\ p &= p^{(0)} + \beta p^{(1)} + \beta^2 p^{(2)} + \dots. \end{aligned} \right\} \quad (5.2)$$

Using (3.10b), we find that the physical azimuthal velocity component is given by the perturbation expansion

$$u_{\varphi} = u_{\hat{\phi}} + \beta \frac{\hat{\sigma}}{a} u_x = \beta \left(u_{\hat{\phi}}^{(1)} + \frac{\hat{\sigma}}{a} u_x^{(0)} \right) + \beta^2 \left(u_{\hat{\phi}}^{(2)} + \frac{\hat{\sigma}}{a} u_x^{(1)} \right) + \dots. \quad (5.3)$$

All velocities are required to be zero around the tube contour. In the case of a circular tube, and only then, the only non-zero perturbation field is $u_{\hat{\phi}}^{(1)} = -(\hat{\sigma}/a)u_x^{(0)}$. Substituting the preceding expressions in the governing equations (3.24), (3.26) and (3.28), we derive a sequence of problems.

The zero-order axial velocity field satisfies the equations of unidirectional tube flow with a linear pressure field, $p^{(0)} = -G\hat{x}$,

$$\hat{\nabla}^2 u_x^{(0)} = -\frac{G}{\mu}, \quad (5.4)$$

where $\hat{\nabla}^2 = \partial^2/\partial\hat{y}^2 + \partial^2/\partial\hat{z}^2$ is the Laplacian in the (\hat{y}, \hat{z}) -plane defined such that $\hat{y} = \hat{\sigma} \cos \hat{\phi}$ and $\hat{z} = \hat{\sigma} \sin \hat{\phi}$. A finite-element method with quadratic six-node triangular elements with curved edges was implemented for solving the Poisson equation (5.4) (e.g. Pozrikidis 2005). Sample results for a circular tube with $n = 3$ sinusoidal corrugations of amplitude $b/a = 0.2$ computed with 1024 elements, for a square tube computed with 512 elements, and for a circular tube with a helical internal partition computed with 1024 elements, are shown in figure 5.

The first-order field satisfies the equations

$$\frac{1}{\mu} \frac{\partial p^{(1)}}{\partial \hat{\sigma}} = \frac{\partial}{\partial \hat{\sigma}} \left(\frac{1}{\hat{\sigma}} \frac{\partial}{\partial \hat{\sigma}} (\hat{\sigma} u_{\hat{\sigma}}^{(1)}) \right) + \frac{1}{\hat{\sigma}^2} \frac{\partial^2 u_{\hat{\sigma}}^{(1)}}{\partial \hat{\phi}^2} - \frac{2}{\hat{\sigma}^2} \frac{\partial u_{\hat{\phi}}^{(1)}}{\partial \hat{\phi}} - \frac{2}{a \hat{\sigma}} \frac{\partial u_x^{(0)}}{\partial \hat{\phi}}, \quad (5.5)$$

$$\frac{1}{\mu} \frac{1}{\hat{\sigma}} \frac{\partial p^{(1)}}{\partial \hat{\phi}} = \frac{\partial}{\partial \hat{\sigma}} \left(\frac{1}{\hat{\sigma}} \frac{\partial}{\partial \hat{\sigma}} (\hat{\sigma} u_{\hat{\phi}}^{(1)}) \right) + \frac{1}{\hat{\sigma}^2} \frac{\partial^2 u_{\hat{\phi}}^{(1)}}{\partial \hat{\phi}^2} + \frac{2}{\hat{\sigma}^2} \frac{\partial u_{\hat{\sigma}}^{(1)}}{\partial \hat{\phi}} + \frac{2}{a} \frac{\partial u_x^{(0)}}{\partial \hat{\sigma}} - \frac{\hat{\sigma} G}{\mu a}, \quad (5.6)$$

$$\hat{\nabla}^2 u_x^{(1)} = 0, \quad (5.7)$$

complemented by the continuity equation

$$\frac{1}{\hat{\sigma}} \left(\frac{\partial (\hat{\sigma} u_{\hat{\sigma}}^{(1)})}{\partial \hat{\sigma}} + \frac{\partial u_{\hat{\phi}}^{(1)}}{\partial \hat{\phi}} \right) = 0. \quad (5.8)$$

The solution of (5.7) is $u_x^{(1)} = 0$, which shows that the first-order velocity contributes neither to the axial flow nor to the axial flow rate. This result is consistent with the asymptotic analysis undertaken in §4. In Cartesian coordinates, (\hat{y}, \hat{z}) , equations (5.5) and (5.6) describing the flow in a transverse plane combine into the forced Stokes equation

$$\hat{\nabla} p^{(1)} = \mu \hat{\nabla}^2 \hat{\mathbf{u}}^{(1)} + \mathbf{b}, \quad (5.9)$$

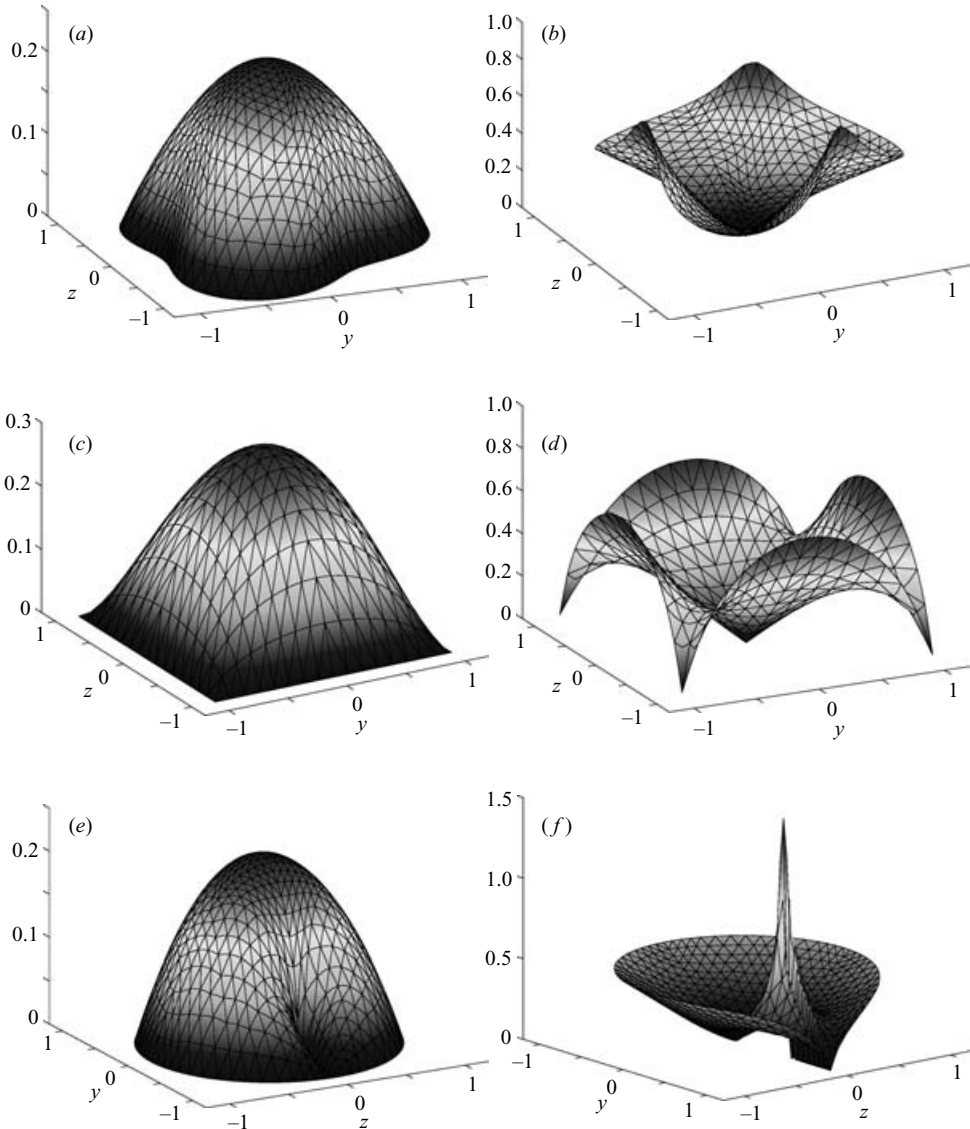


FIGURE 5. (a, b) Unidirectional flow through a circular tube with $n = 3$ sinusoidal corrugations of amplitude $b/a = 0.2$, computed by a finite-element method. (a) Axial velocity field, u_x , and (b) illustration of the magnitude of the velocity gradient, $|\nabla u_x|$. Corresponding results for (c, d) a tube with a square cross-section, and (e, f) a circular tube with a helical internal partition whose edge length is equal to half the tube radius.

where

$$\mathbf{b} = \mu \mathbf{e}_x \times \frac{2}{a} \hat{\nabla} u_x^{(0)} - \frac{\hat{\sigma} G}{a} \mathbf{e}_{\hat{\varphi}}, \tag{5.10}$$

is the body force, \mathbf{e}_x is the unit vector along the x-axis, $\mathbf{e}_{\hat{\varphi}} = (-\hat{z}/\hat{\sigma}, \hat{y}/\hat{\sigma})$ is the unit vector along the $\hat{\varphi}$ axis, $\hat{\mathbf{u}}^{(1)} = (\hat{u}_{\hat{y}}^{(1)}, \hat{u}_{\hat{z}}^{(1)})$, and $\hat{\nabla} = (\partial/\partial \hat{y}, \partial/\partial \hat{z})$ is the gradient in the

(\hat{y}, \hat{z}) -plane. Explicitly,

$$\mathbf{b} = \frac{2\mu}{a} \begin{bmatrix} -\partial u_x^{(0)}/\partial \hat{z} \\ \partial u_x^{(0)}/\partial \hat{y} \end{bmatrix} - \frac{G}{a} \begin{bmatrix} -\hat{z} \\ \hat{y} \end{bmatrix}. \quad (5.11)$$

The continuity equation requires

$$\hat{\nabla} \cdot \hat{\mathbf{u}}^{(1)} = 0. \quad (5.12)$$

The last two equations describe a forced Stokes-flow problem over the tube cross-section, where the body-force term depends on the velocity gradient of the zeroth-order unidirectional flow.

A mixed finite-element method with six-node triangular elements was implemented for solving the first-order flow over the tube cross-section (e.g. Pozrikidis 2005). The velocity was approximated with a quadratic function, and the pressure was approximated with a constant function over each element. The nodal values of the velocity gradient of the unidirectional flow involved in the source term on the right-hand side were computed by averaging the corresponding element values, yielding a smooth gradient field, (figure 5*b, d, f*). In the end, the nodal values of the pressure were computed as averages of adjacent element values with the aid of an appropriate node connectivity table. Sample results for the velocity vector field are shown in figure 6. It is reassuring to observe that the field displayed in figure 6(*a*) is similar in structure to that displayed in figure 3(*a*), even though in this case the parameter $\beta = \pi/3$ is not particularly small. The velocity vector field reveals a core of rotating fluid along the tube centreline for both the circular and the square tubes. The vector field shown in figure 6(*c*) illustrates the effectiveness of the helical fin in inducing a rotational motion centred at the tip of the fin located at $z=0$ and extending from $y/a=0.5$ to 1.

The second-order axial velocity satisfies the Poisson equation

$$\hat{\nabla}^2 u_x^{(2)} + \frac{1}{a^2} \frac{\partial^2 u_x^{(0)}}{\partial \hat{\phi}^2} + \frac{1}{\mu a} \frac{\partial p^{(1)}}{\partial \hat{\phi}} = 0, \quad (5.13)$$

which can be restated in the computationally preferred form

$$\hat{\nabla}^2 u_x^{(2)} - \frac{G}{\mu} \frac{\hat{\sigma}^2}{a^2} - \frac{\hat{\sigma}}{a^2} \frac{\partial}{\partial \hat{\sigma}} \left(\hat{\sigma} \frac{\partial u_x^{(0)}}{\partial \hat{\sigma}} \right) + \frac{1}{\mu a} \mathbf{e}_{\hat{\phi}} \cdot \nabla p^{(1)} = 0. \quad (5.14)$$

The solution was found using the finite-element method discussed earlier in this section for the zeroth-order axial flow. Results of typical calculations for a circular tube with $n = 3$ sinusoidal corrugations, for a tube with a square cross-section, and for a tube with an internal helical fin are shown in figure 7.

The flow rate through a plane normal to the x -axis is given by the perturbation expansion

$$Q = \frac{G\pi a^4}{8\mu} \left[q^{(0)} + \beta^2 q^{(2)} + \dots \right], \quad (5.15)$$

where the dimensionless coefficients $q^{(0)}$ and $q^{(2)}$ are evaluated by integrating the corresponding axial velocities over the tube cross-section. For a square tube with side length equal to $2a$, computations with 32, 128 and 512 elements yielded, respectively, $q^{(0)} = 1.4252, 1.4314$ and 1.4319 , and $q^{(2)} = 0.1955, 0.2174$ and 0.2261 . The value of $q^{(0)}$ obtained with the most refined grid agrees to shown accuracy with the analytical series solution (e.g. Pozrikidis 1997, p. 187). These data demonstrate that the convergence

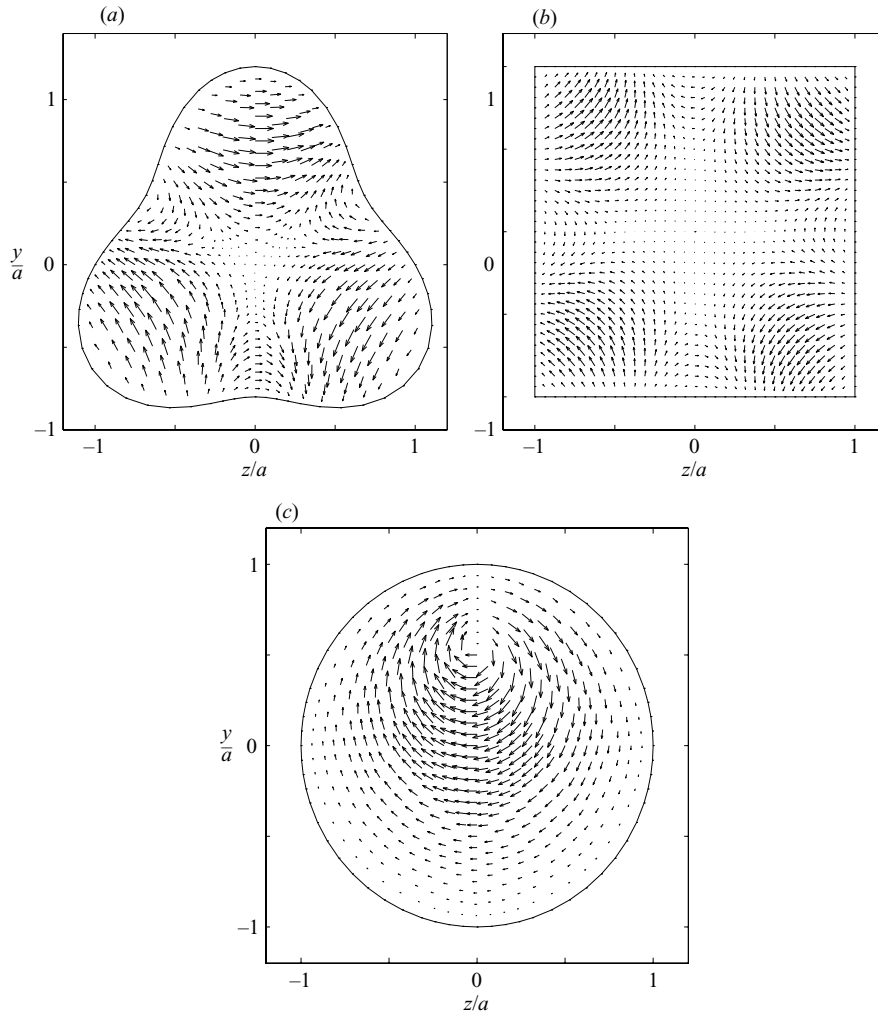


FIGURE 6. First-order velocity vector field in an axial plane for the three cross-sectional geometries described in figure 5.

of $q^{(0)}$ or $q^{(2)}$ with respect to the number is, respectively, quadratic or linear. As expected, $q^{(2)}$ is negative, and this confirms that twisting a tube reduces the flow rate for a fixed pressure gradient.

The perturbation analysis of §2 reveals that, for a circular tube of radius a with sinusoidal corrugations of small amplitude b , $q^{(0)} \simeq 1 - \epsilon^2(2n - 3)$, where $\epsilon = b/a$. Table 1 gives computed values of $q^{(0)}$ and $q^{(2)}$ for selected values of n and ϵ . The numbers in parentheses, representing the predictions of the perturbation solution for small amplitudes, are very close to those corresponding to the finite-element solution. Note that $q^{(0)}$ for $n = 1$ is greater than unity, which means that the flow rate is greater than that predicted by the Poiseuille law based on the mean tube radius, as discussed in §4. In all cases, the value of $q^{(2)}$ is negative.

To establish the range of validity of the perturbation expansion with respect to the pitch parameter β , in figure 8 we plot the dimensionless flow rate $q \equiv 8\pi Q / (G\pi a^4)$

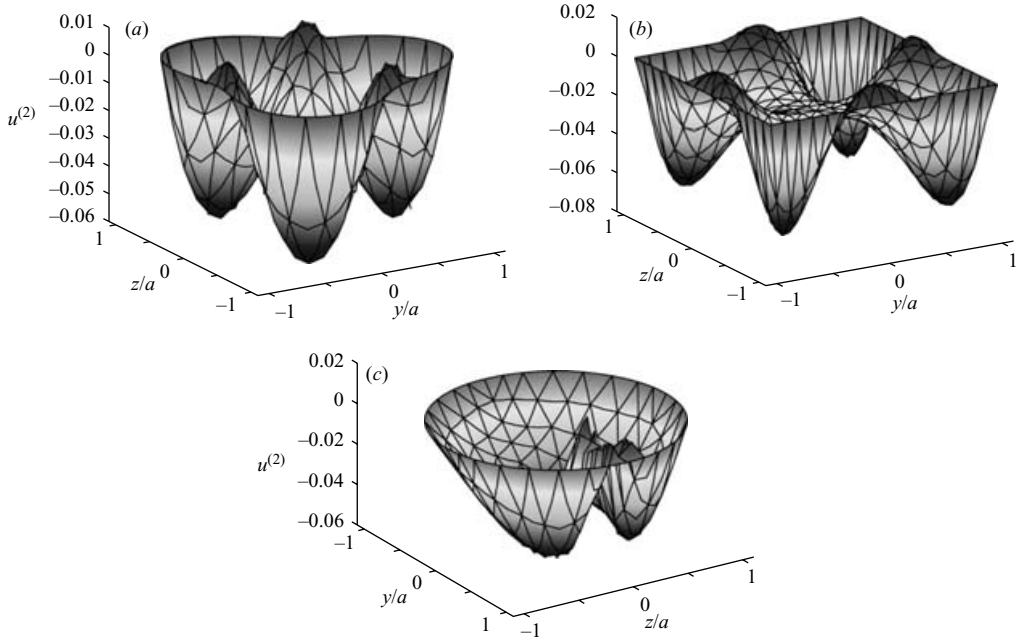


FIGURE 7. Second-order axial velocity field for the three cross-sectional geometries described in figure 5.

n	b/a	$q^{(0)}$	$q^{(2)}$
1	0.10	1.0100 (1.0100)	-0.0185
1	0.20	1.0402 (1.0400)	-0.0746
1	0.25	1.0630 (1.0625)	-0.1175
2	0.10	0.9902 (0.9900)	-0.0439
2	0.20	0.9629 (0.9600)	-0.1620
2	0.25	0.9444 (0.9375)	-0.2393
3	0.10	0.9708 (0.9700)	-0.0676
3	0.20	0.8924 (0.8800)	-0.2198
3	0.25	0.8414 (0.8125)	-0.2994

TABLE 1. The flow rate coefficients $q^{(0)}$ and $q^{(2)}$ for a circular tube of radius a with wavy corrugations of amplitude b . The entries in parentheses represent the predictions of the perturbation solution for small-amplitude corrugation

against ka for several combinations of the reduced amplitude, b/a , and azimuthal wavenumber, n . The solid lines represent the predictions of the large-pitch analysis conducted in this section, and the dotted lines represent the predictions of the small-amplitude analysis conducted in §4. The comparison shows that the second-order large-pitch analysis is accurate approximately when $ka < 2$ or $L > \pi$, that is, when the pitch is longer than approximately three tube radii, and over-predicts the flow rate for a given pressure gradient for shorter wavelengths.

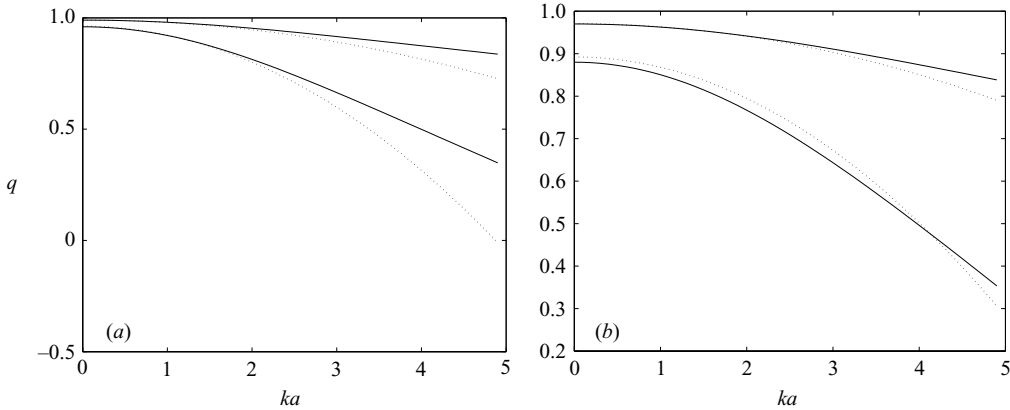


FIGURE 8. Flow in a circular tube of radius a with sinusoidal corrugations of amplitude b . Graphs of the dimensionless flow rate, q for (a) $n = 2$, and (b) $n = 3$. The uppermost curves are for $b/a = 0.1$, and the lower curves are for $b/a = 0.2$. The solid lines represent the predictions of the large-pitch analysis, and the dotted lines represent the predictions of the small-amplitude analysis.

6. Discussion

We have formulated the problem of Stokes-flow through a twisted tube in non-orthogonal helical coordinates, and presented a perturbation solution for a nearly circular tube with sinusoidal corrugations and an asymptotic solution for a tube with arbitrary cross-section and large pitched corrugations. The results in the former case are consistent with those derived by Wang (2006) using an alternative formulation in polar cylindrical coordinates. In addition, we have illustrated the structure of the flow and visualized streamline patterns.

Ideally, the unsimplified Stokes-flow problem would be solved directly by numerical methods. However, the complete formulation results in a coupled system of a two-dimensional forced Stokes-flow problem defined over the tube cross-section and a forced Poisson equation for the axial flow, whose solution defies standard procedures. Fortunately, we have found that the second-order asymptotic solution for large pitch is adequate for predicting the pressure drop under an extended range of conditions. Accounting for the effects of inertia at arbitrary Reynolds numbers requires consideration of an intimidating system of three nonlinearly coupled equations.

The present problem formulation in helical coordinates is also suitable for studying flow in a single-screw extruder. In that case, the zeroth-order problem for infinite pitch describes two-dimensional flow over a cross-sectional plane, while the first-order problem describes axial flow. Numerical solutions of the full three-dimensional problem have been presented in the applied literature using commercial finite-element codes. The proper investigation of the extrusion problem taking into account the helical symmetry was undertaken by Blyth & Pozrikidis (2006).

I am indebted to Haoxiang Luo for illuminating discussions. This research was supported by a grant awarded by the National Science Foundation.

REFERENCES

ARIS, R. 1962 *Vectors, Tensors, and the Basic Equations of Fluid Mechanics*. Prentice-Hall.

- BERGER, S. A., TALBOT, L. & YAO, L.-S. 1983 Flow in curved pipes. *Annu. Rev. Fluid Mech.* **15**, 461–512.
- BLYTH, M. G. & POZRIKIDIS, C. 2006 Stokes flow in a single-screw extruder. Submitted.
- DEAN, W. R. 1927 Note on the motion of fluid in a curved pipe. *Phil. Mag.* (7) **4**, 208–223.
- DEAN, W. R. 1928 The streamline motion of fluid in a curved pipe. *Phil. Mag.* (7) **5**, 673–695.
- EUSTICE, J. 1910 Flow of water in curved pipes. *Proc. R. Soc. Lond. A* **84**, 107–118.
- EUSTICE, J. 1911 Experiments of streamline motion in curved pipes. *Proc. R. Soc. Lond. A* **85**, 119–131.
- GALAKTIONOV, O. S., AN DERSON, P. D., PETERS, G. W. M. & MEIJER, H. E. H. 2001 Optimization of Kenics static mixers. *Computers Fluids* **30**, 271–289.
- GARIMELLA, S. & CHRISTENSEN, R. N. 1995 Heat transfer and pressure drop characteristics of spirally fluted annuli: Part I – Hydrodynamics. *Trans. ASME J. Heat Transfer* **117**, 54–60.
- GARIMELLA, S. & CHRISTENSEN, R. N. 1995b Heat transfer and pressure drop characteristics of spirally fluted annuli: Part II – Heat transfer. *Trans. ASME J. Heat Transfer* **117**, 61–68.
- GERMANO, M. 1982 On the effect of torsion on a helical pipe flow. *J. Fluid Mech.* **125**, 1–8.
- GERMANO, M. 1989 The Dean equations extended to a helical pipe flow. *J. Fluid Mech.* **203**, 289–305.
- HÜTTL, T. J. & FRIEDRICH, R. 2001 Direct numerical simulation of turbulent flows in curved and helically coiled pipes. *Computers Fluids* **30**, 591–605.
- LIU, S. & MASLIYAH, J. H. 1993 Axially invariant laminar flow in helical pipes with a finite pitch. *J. Fluid Mech.* **251**, 315–353.
- MANOUSSAKI, D. & CHADWICK, R. S. 2000 Effects of geometry on fluid loading in a coiled cochlea. *SIAM J. Appl. Maths* **61**, 369–386.
- POZRIKIDIS, C. 1997 *Introduction to Theoretical and Computational Fluid Dynamics*. Oxford University Press.
- POZRIKIDIS, C. 2005 *Introduction to Finite and Spectral Element Methods Using Matlab*. Chapman & Hall/CRC.
- RAINIERI, S., FARINA, A. & PAGLIARINI, G. 1996 Experimental investigation of heat transfer and pressure drop augmentation for laminar flow in spirally enhanced tubes. *Proc. Second Eur. Thermal-Sciences Conf. (EUROTHERM)* Roma (29–31 May 1996).
- RENNIE, T. J. 2004 Numerical and experimental studies of a double-pipe helical heat exchanger. PhD thesis. McGill University, Montreal.
- TUNG, T. T. & LAURENCE, R. L. 1975 A coordinate frame for helical flows. *Polym. Engng Sci.* **15**, 401–405.
- TUTTLE, E. R. 1990 Laminar flow in twisted pipes. *J. Fluid Mech.* **219**, 545–570.
- WANG, C. Y. 1981 On the low-Reynolds-number flow in a helical pipe. *J. Fluid Mech.* **108**, 185–194.
- WANG, C. Y. 2006 Effect of helical corrugations on low-Reynolds-number flow in a tube. *AIChE J.* **52**, 2008–2012.
- WANG, J.-W. & ANDREWS, J. R. G. 1995 Numerical simulation of flow in helical ducts. *AIChE J.* **41**, 1071–1080.
- WITHERS, J. G. & HABDAS, E. P. 1974 Heat transfer characteristics of helical-corrugated tubes for in-tube boiling of refrigerant R-12. *AIChE Symp. Ser.* **70**(138), 98–106.
- YU, Q. & HU, G.-H. 1997 Development of a helical coordinate system and its application to analysis of polymer flow in screw extruders, Part I. The balance equations in a helical coordinate system. *J. Non-Newtonian Fluid Mech.* **69**, 155–167.
- XIE, D. G. 1990 Torsion effect on secondary flow in helical pipe a helical pipe. *Intl J. Heat. Fluid Flow* **11**, 114–119.